ELSEVIER

Chemical Physics 283 (2002) 153–169

Chemical Physics

www.elsevier.com/locate/chemphys

The structure of phenol in the S_1-state determined by high resolution UV-spectroscopy

Christian Ratzer, Jochen Küpper[1], Daniel Spangenberg[2], Michael Schmitt *

Institut für Physikalische Chemie Universitätsstraße 26.43.02, Düsseldorf University, D-40225 Düsseldorf, Germany

Received 31 January 2002

Abstract

The structure of phenol in the electronically excited S_1-state has been examined by rotationally resolved UV-spectroscopy of different isotopomers of phenol. The geometry has been fit to the inertial parameters of 12 isotopomers, using different *pseudo-Kraitchman* fitting strategies. The resulting r_0, r_s, $r_m^{(1)}$, and $r_m^{(2)}$ structures, which differ in the amount of consideration of vibrational effects, will be compared among one another as well as to the results of published ab initio studies. The geometry of the -COH substructure has been determined separately for both electronic states by applying Kraitchman's equations. Independent of the fitting strategy we found a shortening of the CO bond, an increase of the OH bond length and an expansion of the aromatic ring upon electronic excitation. The internal rotation of the hydroxy group causes line splittings that could be observed in the case of the OH species, but remained unresolved for all OD isotopomers. The S_1-state lifetimes of the different isotopomers are shown to depend mainly on the presence of the OH function and depend less on the exchange of CH by CD. Thus, the OH stretching mode is most likely the dominant accepting mode, responsible for the rapid internal conversion in phenol.

1. Introduction

Electronic excitation of aromatic molecules is always accompanied by a change of the geometry of the molecule, reflecting the altered electronic surrounding. In most cases the lowest lying electronic transitions in aromatic molecules are of $\pi^* \leftarrow \pi$-type, causing a lowered bond order in the excited aromatic system and therefore generally causing an expansion of the aromatic ring. In case of substituted aromatics the electronic influence of the substituent plays an important role and has to be considered. Because of the large influence of the substituent on the reactivity of the aromatic, the determination of structures of electronically excited aromatics provides a key also for the examination of their dynamical behavior.

In the last few years hydrogen bonded clusters of phenol with different solvent molecules like water, alcohols, and amines etc. have found growing interest as more or less simple model

* Corresponding author. Fax: +49-211-311-3285.
E-mail address: mschmitt@uni-duesseldorf.de (M. Schmitt).
[1] Present address: University of North Carolina, Department of Chemistry, Chapel Hill, NC 27599, USA.
[2] Present address: Bruker-Daltonik GmbH, 28359 Bremen, Germany.

0301-0104/02/$ - see front matter
PII: S0301-0104(02)00591-8

systems for hydrogen bonding and solvation of aromatic molecules [1–18]. The determination of the structure of such aggregates from their rotational constants demands for an exact knowledge of the respective monomer geometries. Cvitaš et al. [19–22] deduced structural changes upon electronic excitation of several mono- and disubstituted benzenes from their rotational band contours in the electronic spectra. For phenol Christoffersen et al. [23] calculated a shortening of the CO bond of 4.4 pm and an increase in the $C_6C_1C_2$ angle of 3.7° using the rotational constants, obtained from a band contour analysis. Humphrey and Pratt [24] determined the structural change of hydroquinone (*p*-dihydroxybenzene) upon electronic excitation using rotationally resolved LIF spectroscopy. From the rotational constants of three isotopomers they deduced a quinoidal structure in the S_1-state.

For a multitude of isolated molecules their structures in the electronic ground state – generally their r_s-structures – have been investigated by microwave (MW) spectroscopy of isotopically substituted species. Regarding the high resolution of MW spectroscopy a mixture of isotopomers in their natural abundance can be utilized and usually only few pure isotopically substituted substances have to be used. Unfortunately, rotationally resolved UV spectroscopy lacks this ultra high resolution, so that the isotopically substituted species must be bought, what is expensive, or synthesized, what is laborious. For this reason only few studies on the r_s-structures of electronically excited aromatics have been performed.

The complete r_s-structure of phenol in the electronic ground state has been determined by applying Kraitchman's equations using rotational constants from microwave spectroscopy [25]. The rotational constants of h_6-phenol in the S_1-state have been reported by Berden et al. [6] and for [7-D]phenol by Helm and Neusser [26]. In the following publication, the structure in the S_1-state will be examined using parameters determined from rotationally resolved LIF spectroscopy of 12 different isotopomers. We reexamined the two hitherto measured isotopomers, in order to be independent of different Hamiltonians used in the fit.

Electronically excited phenol is known to be a strong acid ($pK_s = 6$) compared to phenol in the electronic ground state ($pK_s = 9.8$) [27]. This increase in acidity by almost four orders of magnitude has been explained by a shift of electron density from the hydroxyl group into the aromatic ring, although more recent theoretical studies point out, that the role of the deprotonated phenolate is more important, than electronic effects in the protonated species [27].

The structure of phenol in the electronically excited S_1-state has been examined theoretically by different groups using the Complete Active Space Self Consistent Field (CASSCF) method with an active space of eight electrons in seven orbitals (CAS(8,7)) [28] and of eight electrons in nine orbitals (CAS(8,9) [29,30]. Furthermore a combined theoretical/experimental work has been published in which a comparison of a Franck–Condon analysis of dispersed fluorescence spectra, obtained via different vibronic levels, with the results of ab initio calculations is performed [31].

In the following we will deduce the structure of phenol in the electronically excited state using different models for the geometry and different fitting strategies and compare them to the structure predicted by ab initio theory.

2. Experimental

2.1. High resolution laser induced fluorescence

The experimental setup for the rotationally resolved LIF is described elsewhere [16]. Briefly, it consists of a ring dye laser (Coherent 899-21) operated with Rhodamine 110, pumped with 6 W of the 514 nm line of an Ar^+-ion laser (Coherent Innova 100). The light is coupled into an external folded ring cavity (LAS WaveTrain) [32] for second harmonic generation (SHG). The molecular beam machine consists of three differentially pumped vacuum chambers that are linearly connected by skimmers. The expansion chamber is evacuated by a 8000 l/s oil diffusion pump (Leybold DI 8000), which is backed by a 250 m^3/h roots blower pump (Saskia RPS 250) and a 65 m^3/h rotary pump (Leybold D65B). The sec-

ond chamber serves as buffer chamber and is pumped by a 400 l/s turbo-molecular pump (Leybold Turbovac 361), backed by a 40 m^3/h rotary pump (Leybold D40B), maintaining a chamber pressure below 1×10^{-5} mbar. The third chamber is pumped by a 145 l/s turbo-molecular pump (Leybold Turbovac 151) through a liquid nitrogen trap and backed by a 16 m^3/h rotary pump (Leybold D16B) resulting in a vacuum better than 1×10^{-6} mbar. The molecular beam is crossed at right angles with the laser beam 360 mm downstream of the nozzle. The resulting fluorescence is collected perpendicular to the plane defined by laser and molecular beam by an imaging optics setup consisting of a concave mirror and two plano-convex lenses. The integrated molecular fluorescence is detected by a photo-multiplier tube (Thorn EMI 9863QB) whose output is discriminated and digitized by a photon counter (Stanford Research Systems SR400) and transmitted to a PC (Pentium II/233). Also the UV laser power, the iodine absorption spectrum and the interferometer transmission signal are detected by photo diodes and stored with the spectrum.

2.2. The isotopically substituted substances

The atomic numbering for phenol used in this publication is given in Fig. 1. h_6-phenol (99.5%) was purchased by Riedel de Haen and used without further purification. [7-D]phenol has been prepared by refluxing dried h_6-phenol with an excess of D_2O (Merck, isotopic purity >98.8%) for three times and subsequent removal of water. Isotopic purity of the sample was higher than 95%. The sample of d_6-phenol (isotopic purity 99%) was purchased from Chemotrade and used without further purification. [^{18}O]phenol has been prepared using the method described by Winkel et al. [33]: 4-nitrophenol reacts with H_2[^{18}O] in the presence of *tert*-butoxide to the [^{18}O]-labelled 4-nitrophenol. The resulting nitrophenol was reduced to 4-aminophenol, followed by diazotization and subsequent exchange of the diazo group with hydrogen using hypophosphoric acid. Isotopic purity of the sample was 60%. [^{18}O][7-D]phenol has been synthesized by refluxing [^{18}O]phenol with D_2O with subsequent removal of water. This procedure was performed only once because of the small amount of [^{18}O]phenol available. [1-^{13}C]phenol (isotopic purity >99%) was purchased by Isotec and used without further purification.

[1-^{13}C][7-D]phenol has been synthesized by refluxing [1-^{13}C]phenol with D_2O and subsequent removal of water. Again, this procedure was performed only once because of the small amount of [1-^{13}C]phenol available. [2-D][7-D]phenol, [3-D][7-D]phenol and [4-D][7-D]phenol have been synthesized using the method described by Pedersen and Larsen [34] by reacting the respective bromophenols with *n*-butyllithium in THF at −78 °C and subsequent deuteriolysis with D_2O. [4-D]phenol was obtained by reaction of [4-D][7-D]phenol with H_2O.

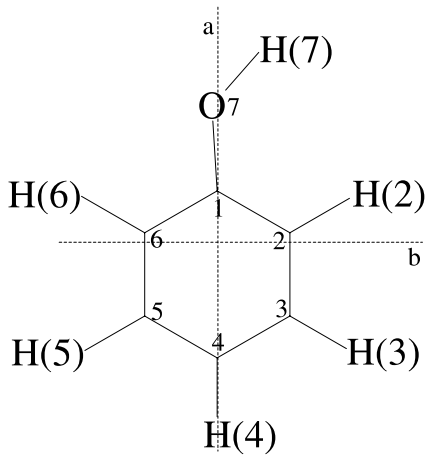

Fig. 1. Atomic numbering and orientation of the principal axis system in phenol. The deviation of the COH group from linearity (cf. Section 3.5.3) is exaggerated for sake of clarity.

3. Results and discussion

The internal rotation of the hydroxyl group causes the 2–3 and the 5–6 side of the molecule (cf. Fig. 1) to be indistinguishable. Therefore phenol has to be described using the molecular symmetry (MS) group G_4. This is also correct for all isotopomers, which are substituted at position 1 or 4, or which are symmetrically ring substituted (2 and 6, 3 and 5, or combinations thereof). The singly

ringdeuterated isotopomers, with the exception of [4-D], exist in two different conformers, with different energies and can be labelled as *cis* and *trans*, regarding the orientation of the hydroxyl group with respect to the substituted position. They have to be classified using the MS group G_2 (or the point group C_s).

The rovibronic spectra of the electronic origins ($\widetilde{A}^1B_2 \leftarrow \widetilde{X}^1A_1$ for G_4 and $\widetilde{A}^1A' \leftarrow \widetilde{X}^1A'$ for G_2) of the 12 isotopically substituted phenols investigated in this study are shown in Figs. 2(a) and (b). All rovibronic spectra exhibit a distinct Q-branch gap and can be classified as *b*-type bands. The rovibronic spectra of the 12 isotopomers are shifted relative to each other, so that their vibronic origins are at zero.

At first sight the spectra can be divided into two classes, regarding the linewidth of the single rovibronic lines. The lines of all [7-H] species are considerably broader than that of the [7-D] species. This can be attributed to a shorter lifetime and to an only partially resolved torsional splitting of the [7-H] isotopomers. Both topics will be discussed later (Sections 3.3 and 3.4).

Three of the rovibronic spectra shown in Figs. 2(a) and (b) are composed of overlapping bands, which are due to different isotopomers [^{18}O]phenol/[^{16}O]phenol, [^{18}O][7-D]phenol/[^{16}O][7-D]phenol, and [3-D][7-D]phenol/[5-D][7-D]phenol). In the following these spectra will be discussed in more detail.

In case of [^{18}O]phenol, the chemical synthesis yielded a mixture of [^{18}O] and [^{16}O]phenol with isotopomeric purity of only 60% for the [^{18}O] isotopomer. Because the electronic origins of [^{18}O]phenol and [^{16}O]phenol are shifted by only 0.1 cm^{-1} their rovibronic bands overlap. The frequency axis in the fourth trace of Fig. 2(a) refers to the [^{18}O]phenol isotopomer. The completely overlapping vibronic origins and the broad spectral lines, which are caused by a short lifetime and an unresolved torsional splitting made the identification of *single* rovibronic lines difficult. Fig. 3 shows the central part of the spectrum in the region of the gap of the *b*-type band with the contributions of both isotopomers together with the fit for both spectra. Comparison of the sum spectrum with the fits of the individual components shows, that some of the lines are completely overlapping within their bandwidth. Therefore the number of lines, which can be used for an assigned fit of the [^{18}O]phenol spectrum is quite small compared to the other isotopomers. However, the relatively large uncertainty of the inertial parameters does not limit the overall reliability of the fit, because the different accuracies of the inertial parameters will be accounted for in the structural determination through the covariance matrices of the parameters. Thus, rotational constants determined with lower precision have a smaller weight on the final structure.

The rovibronic spectra of the overlapping electronic origins of [^{18}O][7-D]phenol and of [^{16}O][7-D]phenol have an even smaller spectral shift of the electronic origins relative to each other, than the undeuterated species. The frequency axis in the fifth trace of Fig. 2(a) refers to the [^{18}O][7-D]phenol isotopomer. Because of the smaller line width of the OD isotopomer it nevertheless was possible to resolve and assign more *single* rovibronic lines than for [^{18}O]phenol. Thus, the uncertainties of the rotational constants of [^{18}O][7-D]phenol are smaller than those of [^{18}O]phenol.

The third spectrum, which shows two overlapping origin bands, due to different isotopomers, namely [3-D][7-D]phenol and [5-D][7-D]phenol is shown in the last trace of Fig. 2(b). The spectral shift between their origins amounts to only 0.5 cm^{-1}. Therefore no Q-branch gap can be observed at first sight in the spectrum. These two isotopomers interconvert rapidly under the experimental conditions of the synthesis, and can therefore not be isolated. Nevertheless the rotational assignment was straightforward utilizing an autocorrelation of the overlapping spectrum. This yields two autocorrelation peaks, whose distance gives immediately the frequency difference of the vibronic origins. With this additional information the two spectra could be separated and assigned easily.

3.1. Vibronic origin frequencies

Since all isotopomers share the same electronic potential energy surface, differences in the vibronic origin frequencies are only due to vibrational zero-

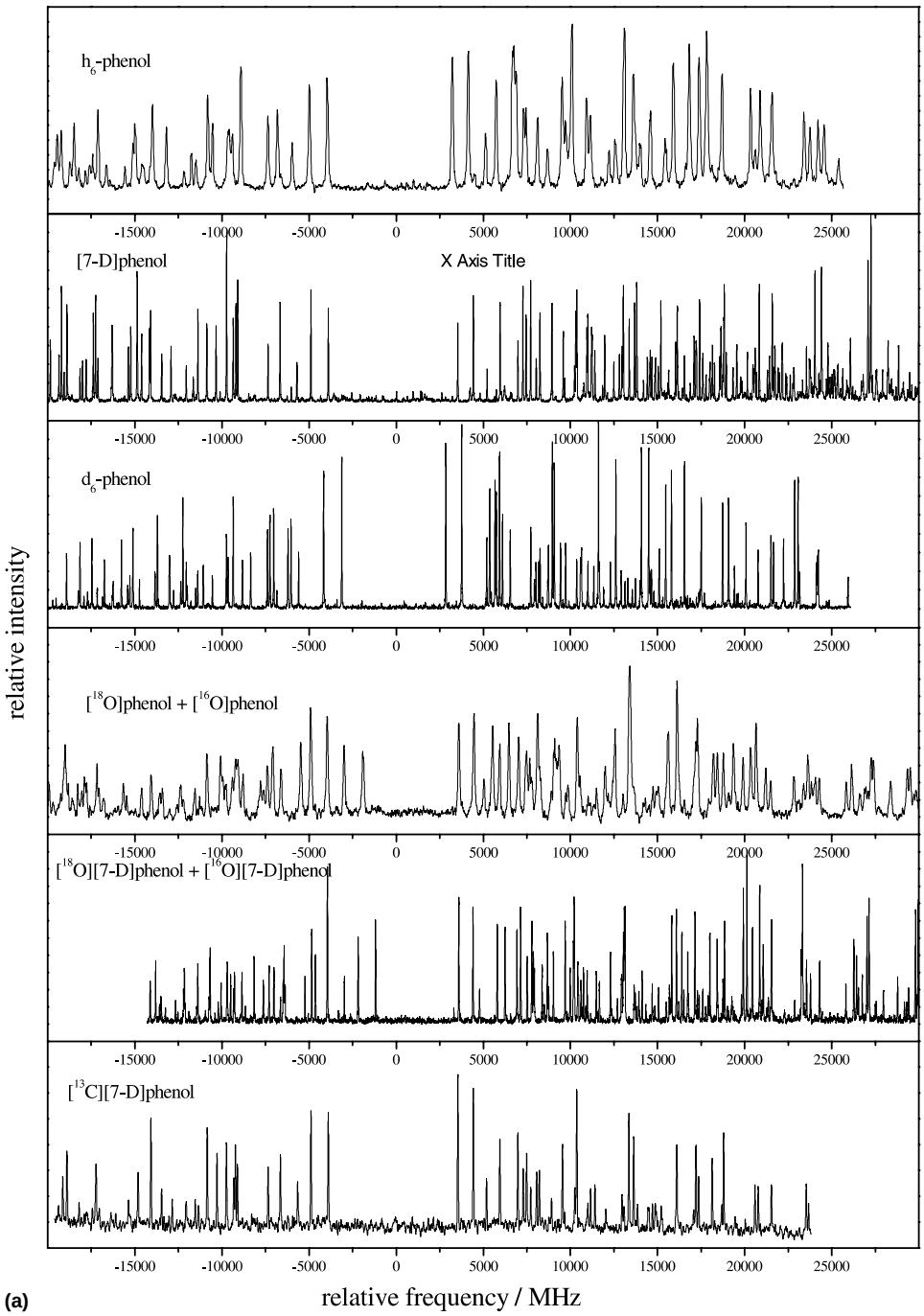

Fig. 2. (a) Rotationally resolved spectra of the electronic origins of h_6-phenol, [7-D]phenol, d_6-phenol, [^{18}O]phenol/[^{16}O]phenol, [^{18}O][7-D]phenol/[^{16}O][7-D]phenol, and [^{13}C][7-D]phenol. The frequency axes in trace four and five refer to the [^{18}O] isotopomers. (b) Rotationally resolved spectra of the electronic origins of [4-D]phenol, [4-D][7-D]phenol, [2-D][7-D]phenol, [6-D][7-D]phenol, [3-D][7-D]phenol and [5-D][7-D]phenol. The spectra are shifted relative to each other so that the vibronic origins are at zero. The frequency axis in the last trace refers to the [3-D][7-D] isotopomer.

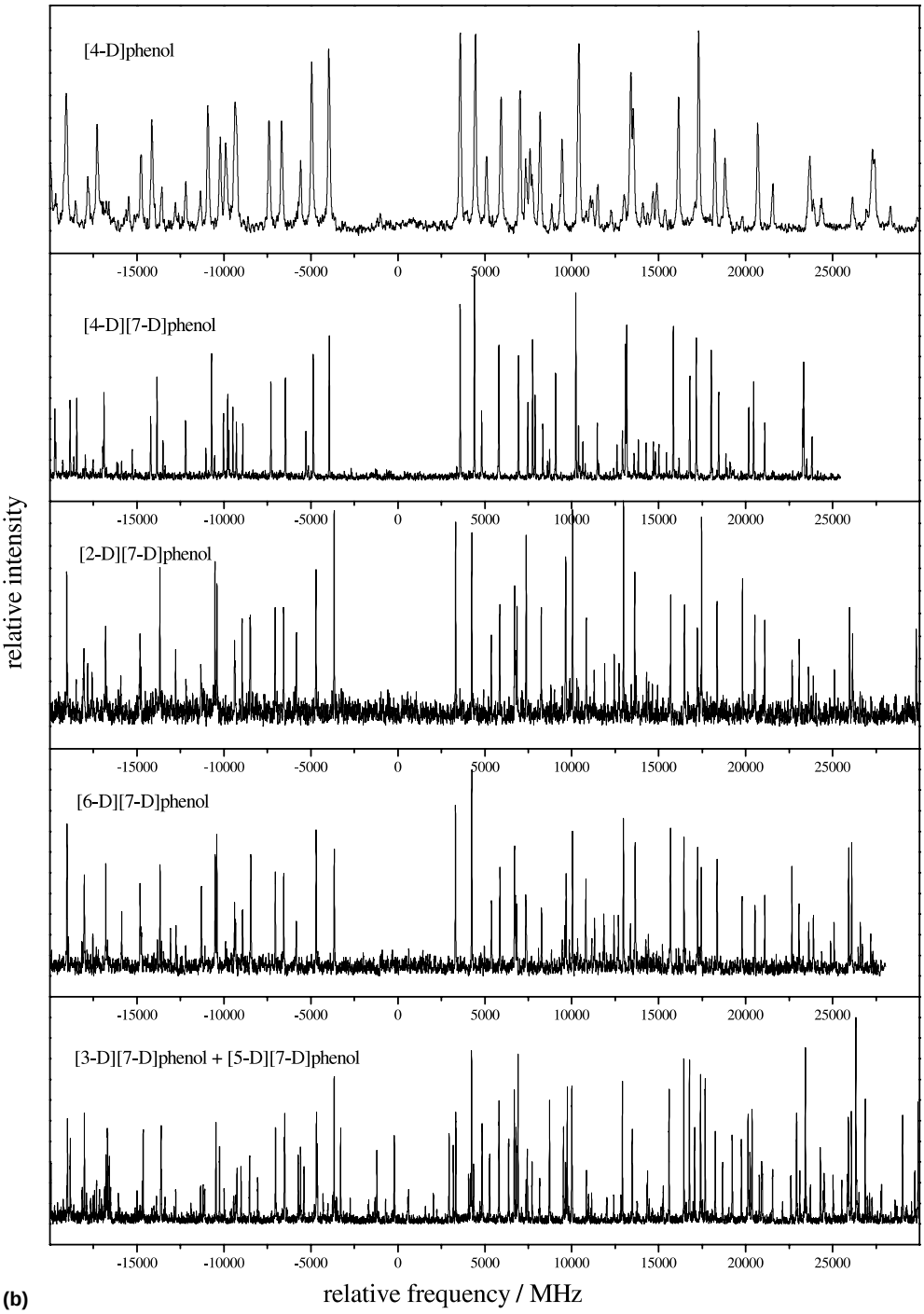

Fig. 2. (*continued*)

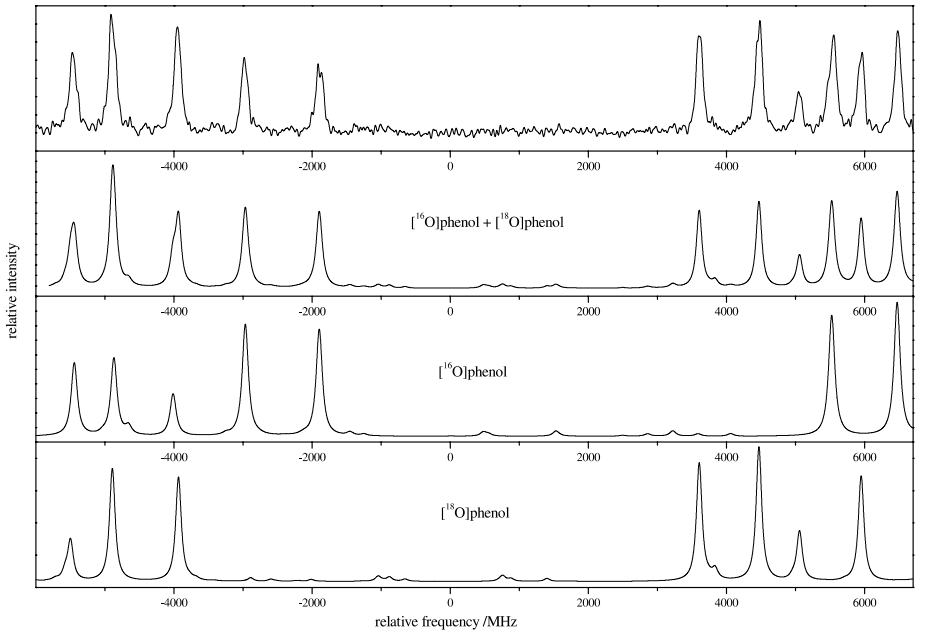

Fig. 3. Central part of the spectra of [^{18}O]phenol/[^{16}O]phenol, together with a simulation of the individual isotopomers, using the inertial parameters from Table 1.

point energy differences between ground and excited state. The vibronic origin frequencies of all isotopomers are given in Table 1; the frequency shifts relative to h_6-phenol are shown in Table 2. The shifts of [2-D][7-D]phenol, [3-D][7-D]phenol, [4-D][7-D]phenol, [5-D][7-D]phenol and [6-D][7-D]phenol, relative to [7-D]phenol are 42.2, 29.4, 24.7, 29.9 and 33.7 cm^{-1} ($\sum = 159.9$ cm^{-1}); the shift of the completely ringdeuterated d_6-phenol amounts to 169.9 cm^{-1} (cf. Table 2). The approximate additivity of the ZPE shifts caused by the CH $\leftrightarrow$ CD exchange, points to a considerable local character of the CH stretching modes in phenol. The high barrier to internal rotation of the OH-group ($V_2 = 1215$ cm^{-1} in the S_0-state and 4710 cm^{-1} in the S_1-state [6]) causes the unsymmetrically 2/6 and 3/5 deuterated isotopomers to be inequivalent. The different zero-point energies of these isotopomers in both electronic states are reflected in their considerably shifted electronic origins. Therefore, it was possible to examine these isotopomers selectively, although they could not be separated chemically. The decision which of the electronic origins belong to which isotopomer has been made by the fit of the geometry to the rotational constants and is described in Section 3.5.2.

3.2. Inertial parameters

All spectra are comprised of pure *b*-type transitions which were fit to a rigid rotor model. The ground state rotational constants of h_6-phenol [35], [4-D]phenol, [7-D]phenol [36], d_6-phenol, and [^{18}O]phenol [37] have been obtained by fitting the published microwave transitions of these isotopomers to a rigid rotor Hamiltonian. This was done to rely on inertial parameters, which were obtained using the same model Hamiltonian for both electronic states. In a subsequent fit of the excited state parameters, the ground state parameters have been constrained to the so obtained values. For all other isotopomers used in this study, no microwave spectra were available and *all* inertial parameters (ground and excited state) have been fitted simultaneously. The accuracy of the ground state parameters obtained from the fit to the MW experiment is about two orders of magnitude higher than of the parameters obtained from a fit

Table 1
Molecular constants of 12 isotopomers of phenol

	h_6-Phenol[a]	[7-D]Phenol[b]	d_6-Phenol[c]	[^{18}O]Phenol[c]
A'' (MHz)	5650.440(55)	5609.321(15)	4654.384(40)	5650.087(6)
B'' (MHz)	2619.205(49)	2528.464(10)	2342.108(31)	2487.333(4)
C'' (MHz)	1789.845(34)	1743.159(9)	1558.383(25)	1727.230(4)
$\Delta I''$ (uÅ^2)	−0.033(4)	−0.050(1)	−0.064(3)	−0.032(1)
A' (MHz)	5313.844(229)	5276.429(47)	4404.560(120)	5313.194(205)
B' (MHz)	2620.315(238)	2531.007(22)	2340.250(41)	2491.973(234)
C' (MHz)	1755.943(126)	1711.598(14)	1529.322(26)	1696.145(128)
$\Delta I'$ (uÅ^2)	−0.165(29)	−0.188(3)	−0.231(7)	0.037(33)
$\tilde{\nu}$ (cm^{-1})	36348.71(1)	36346.90(5)	36518.61(5)	36348.64(5)
$t_{1/2}$ (ns)	2.4 ± 0.3	13.3 ± 1.6	12.5 ± 1.5	2.2 ± 0.4
$\Delta\nu_{sub}$ (MHz)	56 ± 4	–	–	55 ± 5
Lines	27	100	83	33
$S(y)$ (MHz)	7.5	1.8	1.9	10.0
	[7-D][^{18}O]Phenol	[7-D][1-^{13}C]Phenol	[4-D]Phenol[b]	[4-D][7-D]Phenol
A'' (MHz)	5607.182(217)	5608.389(149)	5650.235(3)	5608.051(118)
B'' (MHz)	2407.924(66)	2518.169(66)	2506.187(2)	2420.633(63)
C'' (MHz)	1684.810(71)	1738.162(66)	1736.367(2)	1691.043(42)
$\Delta I''$ (uÅ^2)	−0.050(10)	−0.049(9)	−0.0410(2)	−0.040(7)
A' (MHz)	5274.407(110)	5275.921(126)	5316.580(364)	5275.258(130)
B' (MHz)	2411.944(75)	2520.726(70)	2506.624(129)	2423.183(62)
C' (MHz)	1656.038(54)	1706.814(56)	1705.539(77)	1661.563(45)
$\Delta I'$ (uÅ^2)	−0.175(8)	−0.184(7)	−0.358(18)	−0.203(7)
$\tilde{\nu}$ (cm^{-1})	36346.80(5)	36347.90(5)	36374.96(5)	36373.38(5)
$t_{1/2}$ (ns)	16.7 ± 1.3	12.5 ± 0.7	2.1 ± 0.4	12.6 ± 0.7
$\Delta\nu_{sub}$ (MHz)	–	–	59 ± 4	–
Lines	59	64	44	64
$S(y)$ (MHz)	1.8	2.0	11.1	2.5
	[2-D][7-D]Phenol	[6-D][7-D]Phenol	[3-D][7-D]Phenol	[5-D][7-D]Phenol
A'' (MHz)	5343.102(229)	5335.403(194)	5338.161(166)	5349.789(175)
B'' (MHz)	2519.703(115)	2521.039(128)	2490.353(134)	2487.484(121)
C'' (MHz)	1712.662(101)	1712.387(71)	1698.567(65)	1698.088(76)
$\Delta I''$ (uÅ^2)	−0.072(14)	−0.055(14)	−0.075(13)	−0.019(13)
A' (MHz)	5035.634(174)	5026.591(209)	5028.744(131)	5042.982(193)
B' (MHz)	2520.631(126)	2522.985(123)	2492.041(121)	2487.567(116)
C' (MHz)	1681.138(75)	1681.028(64)	1667.541(78)	1666.963(71)
$\Delta I'$ (uÅ^2)	−0.240(12)	−0.2142(13)	−0.227(14)	−0.203(13)
$\tilde{\nu}$ (cm^{-1})	36390.91(5)	36382.37(5)	36378.13(5)	36378.57(5)
$t_{1/2}$ (ns)	32.5 ± 3.1	12.7 ± 1.7	38.8 ± 7.0	15.6 ± 2.2
$\Delta\nu_{sub}$ (MHz)	–	–	–	–
Lines	59	56	62	61
$S(y)$ (MHz)	2.9	2.4	2.9	1.7

The number of digits retained for each parameter were calculated according to the scheme of Watson [38], so that the calculated line frequencies can be reproduced within 10% of their standard deviation.

[a] The ground state rotational constants have been obtained by fitting the microwave transitions from [35].

[b] The ground state rotational constants have been obtained by fitting the microwave transitions from [36].

[c] The ground state rotational constants have been obtained by fitting the microwave transitions from [37].

to our LIF spectra. The number of digits retained for each parameter in Table 1 were calculated according to the scheme proposed by Watson [38]. Using this number of digits, the line frequencies can be reproduced within 10% of their standard deviation. The uncertainties of the rotational

Table 2
Frequency shifts of the electronic origins of the phenol isotopomers with respect to the origin of h_6-phenol (in cm^{-1}), and changes of the rotational constants (in MHz) and the inertial defects (in u$Å^2$) upon electronic excitation

	h_6	[7-D]	d_6	[^{18}O]	[7-D][^{18}O]	[7-D][1-^{13}C]
$\Delta\nu$ (cm^{-1})	0	−1.8	+169.9	−0.1	−1.9	−0.8
ΔA (MHz)	−336.60	−332.89	−249.82	−336.89	−332.77	−332.47
ΔB (MHz)	+1.11	+2.54	−1.86	+4.64	+4.02	+2.56
ΔC (MHz)	−33.90	−31.56	−29.06	−31.08	−28.77	−31.35
$\Delta\Delta I$ (u$Å^2$)	−0.13	−0.14	−0.17	+0.07	−0.13	−0.14
	[2-D][7-D]	[3-D][7-D]	[4-D][7-D]	[5-D][7-D]	[6-D][7-D]	[4-D]
$\Delta\nu$ (cm^{-1})	+42.2	+29.4	+24.7	+29.9	+33.7	+26.2
ΔA (MHz)	−307.47	−309.42	−332.79	−306.81	−308.81	−333.66
ΔB (MHz)	+0.93	+1.69	+2.55	+0.08	+1.95	+0.44
ΔC (MHz)	−31.52	−31.03	−29.48	−31.13	−31.36	−30.83
$\Delta\Delta I$ (u$Å^2$)	−0.17	−0.15	−0.16	−0.18	−0.16	−0.32

constants are considered by the covariance matrix (see matrix **W** in Eqs. (5) or (7), Section 3.5.1/Fit procedure). The reported standard deviations, given in Table 1, are the square-roots of the diagonal elements of this matrix (the variances).

The resulting molecular parameters for both electronic states are compiled in Table 1. The inertial parameters for ground and excited state will be used later on to deduce the structural changes upon electronic excitation.

Table 2 compiles the changes of the rotational constants upon electronic excitation as obtained from the fit of the spectra of all isotopomers.

3.3. Excited state lifetimes

The S_1-lifetimes for the different isotopomers have been calculated from the Lorentz contributions to the linewidths of single rovibronic lines. They vary between 2.1 ns for [4-D]phenol and 38.8 ns for [3-D][7-D]phenol as can be seen from Table 1.

The isotopomers can roughly be divided into two groups, regarding their lifetimes. Isotopomers with an OH group have a generally much shorter lifetime (around 2 ns) than the OD isotopomers (between 10 and 15 ns), whereas the exchange of all CH by CD as in d_6-phenol does not change the lifetime considerably compared to [7-D]phenol. This is further evidence that the accepting mode for the rapid internal conversion in phenol is the OH stretching vibration, as discussed by Sur and Johnson [2] and Lipert and Colson [39], whereas the effects of the CH stretching vibrations are almost negligible. Surprisingly, the fluorescence lifetimes of [2-D][7-D]phenol (32.5 ns) and [3-D][7-D]phenol (38.8 ns) are by about 20 ns longer than of the other ringdeuterated [7-D]isotopomers, whereas the lifetimes of [5-D][7-D]phenol (15.6 ns) and [6-D][7-D]phenol (12.7 ns) are in the range of all other [7-D]isotopomers. Obviously, the lifetime depends on the *cis*/*trans* position of the C–D with respect to the hydroxy group.

3.4. Torsional splitting and spin statistics

The lineshapes of the rovibrational lines of all [7H] isotopomers are unsymmetrical because of an unresolved torsional splitting (cf. Fig. 4). This was already found to be the case in [^{16}O]phenol [6]. For [^{18}O]phenol a fit of 15 individual lines to two Voigt profiles with a fixed Doppler contribution of 25 MHz, which is the instrumental line width, yielded a Lorentzian line width of 70 ± 10 MHz and a torsional splitting of 55 ± 5 MHz (cf. Fig. 4). The ratio of intensities was not constrained during the fit. Spin statistical consideration lead to the conclusion that the intensity ratio for K_a even:K_a odd should be 10:6 for the $\sigma = 0$ subtorsional component and 6:10 for the $\sigma = 1$ component. The ratio obtained from the fit of the $\sigma = 0$ subtorsional component is 1.7 which agrees well with the theoretical value of $1.\overline{6}$ (10:6). The $\sigma = 0$ subtorsional band is the higher frequency component, thus the transition $211 \leftarrow 202$, shown in Fig. 4 is split into a

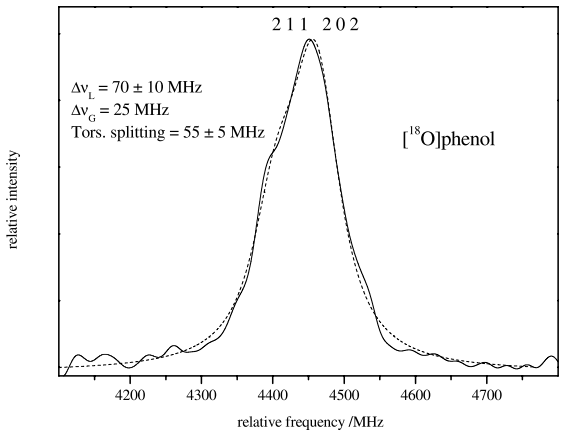

Fig. 4. $211 \leftarrow 202$ Transition in the rovibronic spectrum of [^{18}O]phenol together with a lineshape fit to two Voigt profiles (dashed line). The quoted Lorentzian linewidth contribution and torsional splitting are the mean of 15 independently fitted individual lines in the spectrum.

weaker band at lower frequencies and a stronger band at higher frequencies.

As in the case of [^{18}O] and [^{16}O]phenol the rovibronic lines of [4-D]phenol show a considerable broadening due to the short lifetime and the subtorsional splitting. A lineshape fit gave a Lorentzian contribution to the total line width of 76 ± 5 MHz and a line splitting of the two Voigt components of 59 ± 4 MHz, with the same spin statistical weights as for [^{18}O] and [^{16}O]phenol. Thus, within their uncertainties, the lifetimes and torsional splitting of [^{18}O]phenol, [4-D]phenol and [^{16}O]phenol (taken from [6]) are the same. This can be expected, because the effect of [^{18}O] $\leftrightarrow$ [^{16}O] and [4-H] $\leftrightarrow$ [4-D] exchange on the frequency of the OH stretching vibration, which is supposed to be the accepting mode for a rapid internal conversion is small.[3] The observed torsional splitting is mainly determined by the torsional splitting in the electronic ground state, which changes only little upon the isotopical substitution of the O-atom, as already has been shown by Forest and Dailey [37].

[3] We calculated the frequency difference $\nu(^{16}\mathrm{OH}) - \nu(^{18}\mathrm{OH})$ in the electronic ground state using analytical derivatives at the optimized MP2/6-31G(d,p) geometry to be 12.6 cm^{-1}, which is only 0.3% of the ν_{OH} frequency.

This can be attributed to the fact, that the oxygen atom lies close to the torsional axis and has only little effect on the value of the torsional constant.

The unsymmetrically ringdeuterated isotopomers, belonging to the MS group G_2 do not exhibit nuclear spin statistics. For all [7-D]-substituted species, the subtorsional splitting could not be resolved (cf. Table 1). The torsional splitting in the MW spectrum of [7-D]phenol was experimentally determined to be 0.44 MHz [36]. Thus the splitting between the torsional levels in the ground state is only 0.22 MHz ($\Delta\sigma = \pm 1$), compared to 56 MHz for [7-H]phenol. This is a consequence of the reduced torsional constant F, which amounts 690 GHz for [7-H]phenol [6] and to 345 GHz for [7-D]phenol. Because the splitting of subtorsional levels in the electronically excited state is much smaller, due to the higher barrier, and we observe only the differences of the splitting, the upper limit for the torsional splitting in our experiment is 0.22 MHz. Regarding our instrumentally limited Doppler width of 25 MHz, it is impossible to resolve such a small splitting.

3.5. Determination of the structure

In the following we will denote the calculated structures as ground state structures in a sense of nonexisting vibrational excitation, i.e., excitation of only the vibrationless electronic origin $S_1 \leftarrow S_0$. There exist several models to extract structural data from ground state rotational constants, each resulting in a different degree of approximation with respect to the functional relation of the observable rotational constants B_g^0 to the values B_g^e of the hypothetical equilibrium structure. The subscript g denotes the inertial axes a, b, and c, and the superscripts 0 and e mark zero-point vibrationally averaged constants and equilibrium constants, respectively. All fits, described in the following can be performed on the rotational constants or on the moments of inertia, related by $I_g^0 = h^2/8\pi^2 c B_g^0$ and $I_g^e = h^2/8\pi^2 c B_g^e$.

The simplest approach to the structure is a global fit of the structural parameters of the molecule to the inertial parameters. This completely neglects vibrational effects and implies the approximation

$$I_g^0 = I_g^e(r_0). \quad (1)$$

The resulting structures, derived from (zero-point) vibrationally averaged inertial parameters, are denoted as r_0-structures. These structures largely depend on the isotopomers examined, as has been shown by Costain [40].

The second approach is the use of Kraitchmans equations for individual coordinates in order to obtain the r_s-structure of the molecule [41,40]. Costain showed, that using this method the vibrational effects of the different isotopomers largely cancel, and that the resulting r_s-structures depend little on the isotopomers chosen for the analysis [40]. Implicitly the Kraitchman–Costain method assumes equal vibrational contributions for all isotopomers:

$$I_g^0 = I_g^e(r_s) + \frac{1}{2}\epsilon_{0g}. \quad (2)$$

The ϵ_{0g} contain the average vibrational contributions with respect to the inertial axes g. One problem is, that in general one needs *all* single isotopically substituted species of the parent molecule, which is prohibitive for larger systems. Multisubstitution, as well as different isomeric substitutions at the same positions, can only be included in cases of high symmetry [42].

The third approach is described by Rudolph [43] and results in a *pseudo-Kraitchman* (*p-Kr*) structure (*pseudo-*r_s-structure), which includes the information from all isotopomers simultaneously in a nonlinear fit procedure to inertial parameters as given in Eq. (2). This technique has the advantage, that also multiply substituted isotopomers can be used, in order to obtain the r_s-structure. The first *p-Kr* fits on larger systems were performed by Nösberger et al. [44] on fluoroethane and furan.

Watson [45–48] has introduced the concept of mass-dependent structures, which he designated as $r_m^{(1)}$ and $r_m^{(2)}$-structures. They are obtained by a fit of the structure to the inertial parameters according to

$$I_g^0 = I_g^e\left(r_m^{(1)}\right) + c_g\sqrt{I_g^e\left(r_m^{(1)}\right)} \quad (3)$$

for the $r_m^{(1)}$-structure and by

$$I_g^0 = I_g^e\left(r_m^{(2)}\right) + c_g\sqrt{I_g^e\left(r_m^{(2)}\right)} + d_g\left(\frac{m_1 m_2 \ldots m_N}{M}\right)^{1/(2N-2)} \quad (4)$$

for the $r_m^{(2)}$-structure. In the $r_m^{(1)}$ case no additional parameters have to be fit (the fit of three ϵ_{0g} is replaced by a fit of three c_g) whereas in the $r_m^{(2)}$ case three additional parameters d_g have to be fit. We have written a computer program, *pKrFit*, for a nonlinear fit of the geometry parameters, in internal coordinates, to the inertial constants, applying the four models described above.

3.5.1. Fit procedure

A precondition for any geometry fit of a given molecule based on rotational constants is a mathematical relation between the observed $n = 3k$ rotational constants $B_{g,i}^0$ ($g = a, b, c$; $i = 1, \ldots, k$) or moments of inertia $I_{g,i}^0$ of k isotopomers to the calculated moments of inertia $I_{g,i}^e$ for the equilibrium structure according to one of the described models given in Eqs. (1)–(4). However, the calculated moments of inertia $I_{g,i}^e$ depend on a set of $j = 1, \ldots, m$ independent internal coordinates b_j which describe the equilibrium structure. Thus, we have to connect the observables $B_{g,i}^0$ and the coordinates b_j for any of the $i = 1, \ldots, k$ isotopomers via a relation f which can be expressed as $B_{g,i}^0 = f_i^{[s]}(b_1, \ldots, b_m)$, s characterizing the model (Eqs. (1)–(4)) used.

The coordinates may be given in internal coordinates or Cartesian coordinates. In comparison to Cartesian coordinates the internal coordinates are biased in a sense that parameters may depend on the change of other parameters. This dependency can be removed or minimized by a careful selection of the model. The main advantage of the use of internal coordinates is, that they directly fulfill the three center-of-mass and the three vanishing products-of-inertia conditions and that it is relatively easy to define additional linear constraints among these coordinates. In cases where the number of data points n is less than the number of independent parameters m, one needs to use such constraints in the fit. The constraints applied are presented in the following section.

The aim of the fit is to find the set of internal coordinates $\hat{b}_1, \ldots, \hat{b}_m$ which gives the closest agreement between the measured and the calculated rotational constants $B^0_{g,i}$. It is convenient to introduce the vector $\mathbf{y}$ which collects the n rotational constants, the transpose of this vector being: $\mathbf{y}^{\mathrm{T}} = (B^0_{a,1}, B^0_{b,1}, B^0_{c,1}, \ldots, B^0_{a,k}, B^0_{b,k}, B^0_{c,k})$. In general, the agreement between the vectors of n experimental and computed rotational constants, $\mathbf{y}_{\mathrm{exp}}$ and $\mathbf{y}_{\mathrm{calc}}$, respectively, will be represented by a minimum of a weighted sum of squared residuals $\Delta\mathbf{y} = \mathbf{y}_{\mathrm{exp}} - \mathbf{y}_{\mathrm{calc}}$, i.e.,

$$\chi^2 = \left(\mathbf{y}_{\mathrm{exp}} - \mathbf{y}_{\mathrm{calc}}\right)^{\mathrm{T}} \mathbf{W} \left(\mathbf{y}_{\mathrm{exp}} - \mathbf{y}_{\mathrm{calc}}\right) = \Delta\mathbf{y}^{\mathrm{T}} \mathbf{W} \Delta\mathbf{y}, \tag{5}$$

where the n-by-n positive definite weight matrix $\mathbf{W}$ is the inverse of the covariance matrix of the n experimental rotational constants [49,50]. If we assume that these covariances are dominated by the statistical error represented by the covariances, which were obtained from preceding fits of the rovibrational spectra (see Section 3.2) then $\mathbf{W}$ obviously is a block matrix consisting of k 3-by-3 inverse covariance matrices of the so determined rotational constants. The other extreme position would assume that the fit error is dominated by an average model error. In this case $\mathbf{W}$ can assumed to be a diagonal matrix where each diagonal element has the same (positive) value. We tried both weighting models and found no basic differences in the final results, so that the presented results where performed using the covariances of the rotational constants.

Because of the nonlinear relation $f^{[s]}$ between internal coordinates and rotational constants, containing one of the above mentioned models s = (1), (2), (3), or (4):

$$\mathbf{y}_{\mathrm{calc},i} = f_i^{[s]}(b_1, \ldots, b_m); \quad i = 1, \ldots, n \tag{6}$$

it is necessary to perform a nonlinear fit, which means that starting values for the parameters b_i are needed and an iterative procedure has to be applied. This might possibly lead to different local minima of χ^2, depending on the starting parameter set. We tried several starting geometries, which all converged into the same minimum. Nevertheless, the implementation of a global optimizer despite our local optimizer is necessary to exclude the possible existence of another (deeper) minimum. This will be one of the next projects. Using a Newton-type approximation leads to the unconstrained solution of the m-dimensional step vector $\delta\mathbf{b}^{(r)}$ of the internal coordinates at the rth iteration step [43,50]

$$\Delta\mathbf{b}^{(r)} = \left(\mathbf{J}^{\mathrm{T}}\mathbf{W}\mathbf{J}\right)^{-1}\mathbf{J}^{\mathrm{T}}\mathbf{W}\Delta\mathbf{y}, \tag{7}$$

where $\mathbf{J}$ is the n-by-m Jacobian with the elements $J_{i,j} = \partial f_i^{[s]}(b_1, \ldots, b_m)/\partial b_j$ ($i = 1, \ldots, n$; $j = 1, \ldots, m$). After each step a new set of internal coordinates is created via $\mathbf{b}^{(r)} = \mathbf{b}^{(r-1)} + \Delta\mathbf{b}^{(r)}$ until a minimum of the merit function (5) is found, where $\hat{\mathbf{b}} = \mathbf{b}^{(r)}$.

In the C++ program *pKrFit*,[4] developed to solve these equations, a Levenberg–Marquardt [51,52] variant similar to that proposed by Brandt [50] is used as local minimizer. The algorithm consequently uses orthogonal transforms to solve the equation system (7) which are known to numerically stabilize the solution of nearly singular equation systems (see [44,50] and references therein). All derivatives needed for the calculation of the Jacobian $\mathbf{J}$ where computed as numerical derivatives using forward differences.

Because of the lack of sufficient input data, this minimization procedure was performed under additional ℓ linear constraints ($\ell < m$) among the internal parameters which can generally be expressed as

$$\mathbf{A}\mathbf{b}^{(r)} = \mathbf{d}, \tag{8}$$

where $\mathbf{A}$ is the ℓ-by-m coefficient matrix and the vector $\mathbf{d}$ of length ℓ the right-hand side of these equations. It can be shown, that such a constraint fit can be performed by solving an equation system similar to (7), where the matrix $\mathbf{J}$ is replaced by the product $\mathbf{JZ}$. Here $\mathbf{Z}$ is an m-by-$(m - \ell)$ column-orthogonal matrix computed from the LQ decomposition of the coefficient matrix $\mathbf{A}$; for details see [50,53]. Using *pKrFit* it is possible to express the equations, which define the linear constraints as symbolic equations. They are au-

[4] *pKrFit*, source code available on request.

tomatically transferred into the mathematical form (8) by means of symbolic algebra in our program.

Finally the estimated uncertainties u_j of the $j = 1, \ldots, m$ estimated internal coordinates $\hat{b}_j$ can be computed via the well-known error-propagation formula (see [49,50]) as

$$u_j = \sqrt{\frac{\chi^2}{n-m}}\left[\left(\mathbf{J}^{\mathrm{T}}\mathbf{W}\mathbf{J}\right)^{-1}\right]_{j,j}$$

for any unconstrained fits and as

$$u_j = \sqrt{\frac{\chi^2}{n-(m-\ell)}}\left[\mathbf{Z}\left(\mathbf{Z}^{\mathrm{T}}\mathbf{J}^{\mathrm{T}}\mathbf{W}\mathbf{J}\mathbf{Z}\right)^{-1}\mathbf{Z}^{\mathrm{T}}\right]_{j,j}$$

for the constrained fits. These equations reflect both the relative uncertainties and correlations of the input data via the weight matrix **W** and the average consistency of the model via χ^2.

3.5.2. Overall fit of the structure change upon excitation

Because the number of isotopically substituted phenols is not sufficient to independently determine a complete structure, several restrictions to the model must be made, which are explained in the following. Phenol is assumed to be planar in the electronically excited state. This assumption leaves $2n-3$ internal coordinates for a planar molecule to be determined, which in the case of phenol are 23, still exceeding the number of independent parameters, obtained from the experiment. Thus the number of variables has to be reduced further by some simplifying assumptions for the model used in the fit.

Fig. 1 depicts the model and the atomic numbering we have used. The bond length between C_1 and C_2 has been set equal to the distance between C_6 and C_1. In the same manner $\overline{C_2C_3}$ is set equal to $\overline{C_5C_6}$ and $\overline{C_3C_4}$ is set equal to $\overline{C_4C_5}$. This reduces also the number of independent angles in the fit: $C_1C_2C_3$ is equal to $C_5C_6C_1$ and $C_2C_3C_4$ is equal to $C_4C_5C_6$. All CH distances are treated as being equal, all CCH angles are fixed to a value of $(360° - \mathrm{CCC})/2$, which is the bisector of the external angle of three adjacent C-atoms. Also the sum of internal angles in the benzene hexagon was set to 720°, which of course is true for any hexagon. This imposes six new linear boundary conditions for the nonlinear fit. The $\overline{C_1O}, \overline{OH}$ distances and the C_1OH and C_2C_1O angles are fit. So the number of independent structural parameters used in the fit can be reduced to eleven. We applied all fitting strategies of the geometry to the inertial parameters, as described in Section 3.5. The resulting geometrical structures are denoted as r_0, pseudo-r_s, $r_m^{(1)}$, and $r_m^{(2)}$ structures, as defined in Section 3.5. As a test of the computer program, the previously determined r_s-structure of phenol in the electronic ground state has been compared to a *pseudo-Kraitchman* fit to the published inertial parameters from MW measurements [25,36,37] using *pKrFit*. The so calculated pseudo-r_s structure is in very good agreement with the r_s-structure given by Larsen [25]. In order to determine the geometry changes upon electronic excitation, for each fitting strategy the ground state geometry must be fit to the same restricted model as is used for the S_1-state.

For the pair [2-D][7-D]phenol/[6-D][7-D]phenol the decision which set of the moments of inertia parameters belongs to which isotopomer is not unambigious. However, an unique assignment can be given, based upon the quality of the structure fit. The same holds true for the pair of isotopomers [3-D][7-D]phenol/[5-D][7-D]phenol. With the assignment of the isotopomers as given in Table 1 stable fits could be obtained, which depend very little on the starting geometry chosen. The resulting structural parameters for our model are given in Tables 3 and 4, respectively.

None of the geometries for the electronically excited state, given in Table 3 does support the assumption of a quinoidal distortion of the aromatic ring in the S_1-state [6]. Up to now, only the C_1-atom of the aromatic ring has been isotopically substituted. This reduces the accuracy for the coordinates of the C-atoms in the ring. Further work on the missing ^{13}C isotopomers, which will improve the quality of the fit and present the possibility to perform a complete Kraitchman–Costain analysis, is on the way. Nevertheless, the current results strongly suggest an aromatic and not a quinoidal excited state.

Table 3
r_0, r_s, $r_m^{(1)}$, and $r_m^{(2)}$ structural parameters of the electronically excited S_1-state of phenol

	r_0	Pseudo-r_s	$r_m^{(1)}$	$r_m^{(2)}$
C_1–C_2 (Å)	1.4418(251)	1.4471(140)	1.4368(242)	1.4321(236)
C_2–C_3 (Å)	1.4525(94)	1.4532(58)	1.4672(154)	1.3834(242)
C_3–C_4 (Å)	1.4218(49)	1.4225(19)	1.4113(211)	1.3993(233)
C_1–O (Å)	1.3264(170)	1.3246(89)	1.3271(101)	1.3440(92)
O–H (Å)	0.99221(522)	0.9897(293)	0.9882(320)	0.9697(265)
C–H (Å)	1.071(3)	1.072[a]	1.0727(58)	1.0732(54)
C_1–O–H (°)	107.51(313)	109.77(191)	109.25(205)	109.20(169)
C_1–C_2–O (°)	119.788(1.451)	119.84(80)	119.76(86)	120.22(68)
C_1–C_2–C_3	118.283(0.359)	118.57(22)	118.55(24)	119.43(30)
C_2–C_3–C_4	117.988(378)	118.31(23)	118.31(26)	119.21(32)
C_1–C_2–H_2	123.728(710)	123.12(44)	123.14(49)	121.36(61)
ϵ_A/c_A	–	0.7745(3620)	0.1735(2600)	0.4542(2902)
ϵ_B/c_B	–	−3.1377(12930)	−0.1773(2039)	−0.0164(1710)
ϵ_C/c_C	–	−2.7768(12661)	−0.0596(2945)	0.1264(2426)
d_A	–	–	–	0.0703(1308)
d_B	–	–	–	2.1695(5997)
d_C	–	–	–	3.2272(9445)

[a] This parameter has not been fit due to numerical instabilities and was varied manually.

Table 4
r_0, r_s, $r_m^{(1)}$, and $r_m^{(2)}$ structural parameters of the electronic ground state S_0 of phenol

	r_0	Pseudo-r_s	$r_m^{(1)}$	$r_m^{(2)}$
C_1–C_2 (Å)	1.3827(745)	1.4187(139)	1.4298(142)	1.4061(309)
C_2–C_3 (Å)	1.4021(192)	1.3912(34)	1.4075(50)	1.3849(447)
C_3–C_4 (Å)	1.3991(172)	1.3931(24)	1.3957(70)	1.4047(81)
C_1–O (Å)	1.3686(332)	1.3562(55)	1.3482(50)	1.3612(108)
O–H (Å)	0.9619(257)	0.9483(45)	0.9458(43)	0.9549(109)
C–H (Å)	1.0792(57)	1.085[a]	1.0796(21)	1.0763(26)
C_1–O–H (°)	107.84(417)	110.087(780)	110.62(70)	108.53(137)
C_1–C_2–O (°)	123.26(444)	121.49(75)	121.10(66)	122.94(128)
C_1–C_2–C_3	120.23(123)	120.27(19)	120.25(16)	120.60(46)
C_2–C_3–C_4	119.70(159)	119.86(27)	119.87(23)	120.18(48)
C_1–C_2–H_2	120.07(134)	119.86(28)	119.88(23)	119.21(90)
ϵ_A/c_A	–	1.4072(2082)	0.0476(712)	−0.0133(938)
ϵ_B/c_B	–	0.0782(650)	−0.1258(824)	−0.0919(1039)
ϵ_C/c_C	–	1.4057(611)	−0.0810(1041)	−0.0706(1322)
d_A	–	–	–	0.0752(460)
d_B	–	–	–	0.6681(11219)
d_C	–	–	–	0.5933(11100)

[a] This parameter has not been fit due to numerical instabilities and was kept fixed at the value given by Larsen [25].

3.5.3. Determination of the geometry change of the functional group

The r_s-geometry of the COH group in the electronically excited state has been determined independently from the overall fit of the molecular structure using the Kraitchman–Costain method [41,54]. The rotational constants from Table 1 for [7-D]phenol, [^{18}O][7-D]phenol, [^{13}C][7-D]phenol and [^{18}O]phenol were used to calculate the substitution coordinates. Special attention has to be paid to the coordinates of the O-atom, as Kraitchman's equation yield only the absolute values of the coordinates. Since the center of mass of the OH group lies on the inertial *a*-axis [36] the *b*-coordinate of the oxygen atom must be negative for the convention chosen, cf. Table 5 and Fig. 1.

Because the C_1-atom is close to the *a*-axis, its *b*-coordinate cannot be determined with sufficient accuracy. For the determination of the bond parameters it has therefore been set to zero. From the substitution coordinates, given in Table 5 an increase of the OH bond length of 1.9 pm, a decrease of the CO bond length of 1.5 pm and an increase of the COH angle of 1.0° are calculated (cf. Table 6).

3.6. Comparison to the results of ab initio calculations

We compare the results of our experimental determination of the structural changes upon electronic excitation in phenol to the results of previously published CASSCF studies on phenol, using an active space of eight electrons in nine orbitals [30]. This is to our knowledge up to now the largest active space used for a geometry optimization of phenol in the S_0 and S_1-state.

The most significant structural change from the ab initio calculations is an increase of all C-C bond lengths, i.e., an inflation of the aromatic ring. The $\overline{C_1C_2}$ distance increases by 3.9 pm, $\overline{C_2C_3}$ by 3.2 pm, $\overline{C_3C_4}$ by 4.1 pm, $\overline{C_4C_5}$ by 3.3 pm, $\overline{C_5C_6}$ by 4.2 pm and $\overline{C_6C_1}$ by 2.9 pm, whereas the CH distance decreases slightly by approximately 0.3 pm for each CH-bond. The CO bond length decreases by 1.9 pm, whereas the OH distance does not change upon electronic excitation. Although most of the geometry changes are confirmed by the experiment, the OH bond length is found to be increased between 1.5 and 4.2 pm, depending on the model used for the fit, in sharp contrast to the calculations. Table 7 compares the values for the bond length and angle changes calculated from Tables 3 and 4.

Table 5
Substitution coordinates (in Å) of phenol for both electronic states

	S_0		S_1	
	a	*b*	*a*	*b*
C	0.907(1)	0.123(9)	0.905(3)	0.096(11)
O	2.2114(6)	−0.124(6)	2.1949(7)	−0.128(4)
H	2.586(1)	0.853(2)	2.591(2)	0.864(3)

The substitution chain [7-D]phenol, [^{18}O][7-D]phenol, [^{13}C][7-D]phenol and [^{18}O]phenol is used.

Table 6
Geometry parameters of the COH group of phenol for both electronic states and their changes using the coordinates given in Table 5

	S_0	S_1	Δ
C–O Distance (Å)	1.304(3)	1.289(4)	−0.015
O–H Distance (Å)	0.931(6)	0.950(4)	+0.019
COH Angle (°)	113.7(6)	114.6(7)	+0.9

The *b*-coordinate of the C atom has been set to zero due to its smallness.

4. Conclusions

The geometric structure of phenol in its electronically excited S_1-state has been determined from the inertial parameters of 12 isotopomers. For the two chemically inseparable pairs [2/6-D][7-D]phenol and [3/5-D][7-D]phenol isotopomers it was not obvious which electronic origin belongs to which species. These species differ in the orientation of the OD group relative to the ringdeuterated

Table 7
Comparison of the experimental geometries changes (r_0, pseudo-r_s, $r_m^{(1)}$, and $r_m^{(2)}$) upon electronic excitation with the ab initio based results (r_e)

	r_e[a]	r_s	r_0	Pseudo-r_s	$r_m^{(1)}$	$r_m^{(2)}$
ΔC_1–C_2 (pm)	+3.9	–	+5.9	+2.8	+0.7	+2.6
ΔC_2–C_3 (pm)	+3.2	–	+5.0	+6.1	+0.4	+0.15
ΔC_3–C_4 (pm)	+4.1	–	+2.3	+2.9	+1.6	−0.5
ΔC_1–O (pm)	−1.9	−1.5	−0.5	−3.2	−2.1	−1.7
ΔO–H (pm)	0	+1.9	+3.0	+4.1	+4.2	+1.5
ΔC–H (pm)	−0.03	–	−0.8		−0.7	−0.3
ΔC_1–O–H (°)	+0.2	+0.9	+0.3	−0.3	−1.3	+0.7
ΔC_1–C_2–O (°)	−1.2	–	−3.5	−1.6	−1.3	−2.7

[a] The ab initio values from [30] are given.

position and can be labelled *cis* and *trans*. The existence of two distinguishable isomers is confirmed by their considerably different zero-point energy shifts. From the fit of the structure to the inertial parameters the assignment within these pairs was obvious due to large deviations between the calculated and observed rotational constants for all but one possible assignment. Moreover it can be concluded, that the two *cis*-isotopomers ([2-D][7-D]phenol and [3-D][7-D]phenol) show a significantly longer fluorescence lifetime compared to all other isotopomers. In order to confirm this surprising effect independent lifetime measurements will be performed in the near future.

Several models for determination of the structure of phenol in both electronic states have been applied, which all agree in the fact that the CO bond length decreases, whereas the OH bond length increases upon electronic excitation. This increase is expected because of the increased acidity of phenol in the electronically excited state. The CASSCF calculations do not reproduce this effect, whereas the CO shortening is predicted quite well. This probably is caused by the relatively small active space employed, not including σ-type orbitals in the OH bond, The individual CC bond lengths of the aromatic ring increase, which also is reproduced at the CASSCF level. Thus, the use of molecular orbitals with exclusively π-symmetry in the CASSCF calculations describes the geometry changes in the aromatic ring satisfactorily, whereas the σ-type OH bond cannot be described well. The extent to which the individual bond length increase, depends on the model used. In principle the $r_m^{(2)}$-model should result in more reliable geometry parameters than the other models, because vibrational effects are included in six additional parameters. Nevertheless, for this model there are three more degrees of freedom in the fit than using the $r_m^{(1)}$- or r_s-models and six more degrees of freedom compared to the plain r_0-structure. The model which appears to be most suitable is the *pseudo*-Kraitchman fit. It slightly exaggerates the shortening of the CO bond, what is compensated by an overestimation of the C_2C_3 bond length increase. Therefore a definite statement about the absolute distortion of the aromatic ring upon electronic excitation has to be postponed until further work on [^{13}C] substituted species (or other isotopomers, in order to increase the degrees of freedom in the fit) has been performed, but the current work suggests a breathing-like expansion of the aromatic ring and no quinoidal distortion.

Overall, the experimentally determined structural changes intuitively agree with the strongly enhanced acidity of phenol in its excited singlet state. Moreover many details of the changes in the nuclear framework were determined.

Acknowledgements

This work was made possible by the support of the Deutsche Forschungsgemeinschaft (SCHM 1043/9-2). We gratefully acknowledge the support of Prof. Dr. Karl Kleinermanns. We wish to thank Christian Plützer and Isabel Hünig for supporting us with the R2PI data for the electronic origins of several isotopomers and Arnim Westphal and Arno Reichelt for the preparation of some isotopically substituted phenols.

References

[1] H. Abe, N. Mikami, M. Ito, J. Phys. Chem. 86 (1982) 1768.
[2] A. Sur, P.M. Johnson, J. Chem. Phys. 84 (1986) 1206.
[3] R.J. Stanley, A.W. Castleman Jr., J. Chem. Phys. 94 (1991) 7744.
[4] R.J. Lipert, S.D. Colson, J. Chem. Phys. 89 (1988) 4579.
[5] M. Schütz, T. Bürgi, S. Leutwyler, T. Fischer, J. Chem. Phys. 98 (1993) 3763.
[6] G. Berden, W.L. Meerts, M. Schmitt, K. Kleinermanns, J. Chem. Phys. 104 (1996) 972.
[7] M. Gerhards, M. Schmitt, K. Kleinermanns, W. Stahl, J. Chem. Phys. 104 (1996) 967.
[8] M. Schmitt, C. Jacoby, K. Kleinermanns, J. Chem. Phys. 108 (1998) 4486.
[9] R.M. Helm, H.P. Vogel, H.J. Neusser, J. Chem. Phys. 108 (1998) 4496.
[10] T. Ebata, M. Furukawa, T. Suzuki, M. Ito, J. Opt. Soc. Am. B 7 (1990) 1890.
[11] O. Dopfer, K. Müller-Dethlefs, J. Chem. Phys. 101 (1994) 8508.
[12] T. Watanabe, T. Ebata, S. Tanabe, N. Mikami, J. Chem. Phys. 105 (1996) 408.
[13] S. Tanabe, T. Ebata, M. Fujii, N. Mikami, Chem. Phys. Lett. 215 (1993) 347.

[14] A. Courty, M. Mons, B. Dimicoli, F. Piuzzi, V. Brenner, P. Millié, J. Phys. Chem. A 102 (1998) 4890.
[15] E. Cordes, O. Dopfer, T.G. Wright, K. Müller-Dethlefs, J. Phys. Chem. 97 (1993) 7471.
[16] M. Schmitt, J. Küpper, D. Spangenberg, A. Westphal, Chem. Phys. 254 (2000) 349.
[17] J. Küpper, A. Westphal, M. Schmitt, Chem. Phys. 263 (2001) 41.
[18] A. Iwasaki, A. Fujii, T. Watanabe, T. Ebata, N. Mikami, J. Phys. Chem. 100 (1996) 16053.
[19] T. Cvitaš, J. Hollas, Mol. Phys. 18 (1970) 101.
[20] T. Cvitaš, J. Hollas, Mol. Phys. 18 (1970) 793.
[21] T. Cvitaš, J. Hollas, Mol. Phys. 18 (1970) 801.
[22] T. Cvitaš, J. Hollas, G. Kirby, Mol. Phys. 19 (1970) 305.
[23] J. Christoffersen, J.M. Hollas, G.H. Kirby, Proc. R. Soc. A. 307 (1968) 97.
[24] S.J. Humphrey, D.W. Pratt, J. Chem. Phys. 99 (1993) 5078.
[25] N.W. Larsen, J. Mol. Struct. 51 (1979) 175.
[26] R.M. Helm, H.J. Neusser, Chem. Phys. 239 (1998) 33.
[27] G. Granucci, J. Hynes, P. Millié, T.-H. Tran-Thi, J. Am. Chem. Soc. 122 (2000) 12243.
[28] W.H. Fang, J. Chem. Phys. 112 (2000) 1204.
[29] J. Lorentzon, P.-A. Malmqvist, M. Fülscher, B. Roos, Theor. Chim. Acta 91 (1995) 91.
[30] S. Schumm, M. Gerhards, W. Roth, H. Gier, K. Kleinermanns, Chem. Phys. Lett. 263 (1996) 126.
[31] S. Schumm, M. Gerhards, K. Kleinermanns, J. Phys. Chem. A 104 (2000) 10648.
[32] M. Okruss, R. Müller, A. Hese, J. Mol. Spectrosc. 193 (1999) 293.
[33] C. Winkel, M. Aarts, F. van der Heide, E. Buitenhuis, J. Lugtenburg, Recl. Trav. Chim. Pays-Bas 108 (1989) 139.
[34] T. Pedersen, N.W. Larsen, J. Labelled Compd. 5 (1969) 195.
[35] E. Mathier, D. Welti, A. Bauder, H.H. Günthard, J. Mol. Spectrosc. 37 (1971) 63.
[36] T. Pedersen, N.W. Larsen, L. Nygaard, J. Mol. Struct. 4 (1969) 59.
[37] H. Forest, B.P. Dailey, J. Chem. Phys. 45 (1966) 1736.
[38] J.K.G. Watson, J. Mol. Spectrosc. 66 (1977) 500.
[39] R.J. Lipert, S.D. Colson, J. Phys. Chem. 93 (1989) 135.
[40] C. Costain, J. Comp. Phys. 29 (1958) 864.
[41] J. Kraitchman, Am. J. Phys. 21 (1953) 17.
[42] A. Chutjian, J. Mol. Spectrosc. 14 (1964) 361.
[43] H.D. Rudolph, Struct. Chem. 2 (1991) 581.
[44] P. Nösberger, A. Bauder, H.H. Günthard, Chem. Phys. 1 (1973) 418.
[45] J.K.G. Watson, J. Mol. Spectrosc. 48 (1973) 479.
[46] J.G. Smith, J.K.G. Watson, J. Mol. Spectrosc. 69 (1978) 47.
[47] J.K.G. Watson, A. Roytburg, W. Ulrich, J. Mol. Spectrosc. 196 (1999) 102.
[48] J.K.G. Watson, J. Mol. Spectrosc. 207 (2001) 16.
[49] W.C. Hamilton, Statistics in Physical Science, Ronald Press, New York, 1964.
[50] S. Brandt, Data Analysis, third ed., Springer Verlag, Berlin, 1998.
[51] K. Levenberg, Q. Appl. Math. 2 (1944) 164.
[52] D.D. Marquardt, J. Soc. Ind. Appl. Math. 11 (1963) 431.
[53] P.E. Gill, W. Murray, Numerical Methods for Constrained Optimization, Academic Press, London, 1974.
[54] W. Gordy, R.L. Cook, Microwave Molecular Spectra, third ed., Wiley, New York, 1984.